

# Numerical investigation on a combined loop heat pipe and graphite sheets cooling system for automotive applications

M Bernagozzi<sup>1</sup>, A Georgoulas<sup>1</sup>, N Miché<sup>1</sup>, C Rouaud<sup>2</sup> and M Marengo<sup>1</sup>

<sup>1</sup>Advanced Engineering Centre, University of Brighton, Brighton, UK

<sup>2</sup>Ricardo Innovation, plc, Shoreham by Sea, UK

E-mail: [M.Bernagozzi2@brighton.ac.uk](mailto:M.Bernagozzi2@brighton.ac.uk)

**Abstract.** An innovative Battery Thermal Management System for a 3-cell Electric Vehicle module is proposed, involving Loop Heat Pipes and graphite sheets, with the particular aim of fast charging and reacting to automotive requirements. The design feasibility is verified through a Lumped Parameter Model, which has been validated comparing the data from an experimental demonstrator which included a copper/copper flat plate Loop Heat Pipe running ethanol. Results show that this solution is able to maintain the maximum temperature below 32°C after a 10 min fast charge cycle. System performance with a standard working fluid such as ethanol are compared with the system performance using a novel fluid, Novec™ 649, which has desirable features for the automotive industry, such as non-flammability, non-toxicity, below-zero freezing point and outstanding environmental properties (GWP = 1, ODP = 0). Nevertheless, comparison between the results with the two fluids reported no significant difference in thermal performance showing no contraindication in the use of the novel working fluid. Moreover, the model was used to estimate the effect of the Loop Heat Pipe building material, resulting in no sensible difference between the utilization of copper and aluminium, de facto justifying the choice of the lighter material for future applications.

## 1. Introduction

Electric Vehicles (EVs) are emerging as the chosen solution to reduce emissions from passenger cars. Regulations emitted by governments worldwide have pushed automotive OEMs to accelerate in providing novel effective solutions to successfully tackle the long-standing limitations of EVs. These are: high costs, limited all-electric range and long recharging times [1].

The battery pack is the core of the EV. It is directly linked with all three of the abovementioned factors and it is greatly influenced by temperature. Preferably, battery packs should feature a carefully designed Battery Thermal Management System (BTMS), which needs to operate on three levels: *cell level*, maintaining the temperature gradient across the cell between 3-5°C; *module level*, maintaining the temperature between cells within a 5°C difference; finally, *pack level*, as the overall temperature of the cells belonging to the pack needs to be kept between 25°C and 40°C, for maximum performance and operative life. This is due to the strong link between the thermal and chemical behavior of cells, highlighted in several recent studies [2].

Moreover, not only the EV performance is affected by temperature, but safety as well. In fact, a TMS should prevent the onset of the thermal runaway phenomenon, where a self-sustained reaction springs from the melting of the separator (~130°C), leading to smoke, fire and eventually explosion [3].

So far, commercially available EVs are relying on two type of BTMS, i.e. air or liquid cooling. Despite the fact that these two constitute already established technologies, they present some inherit

drawbacks as well as potential for improvement. For instance, air cooling is not efficient enough to keep low temperature during high charging rates and does not provide optimum temperature homogeneity; on the other hand, liquid cooling increases the costs, weight and complexity of the system by adding parts and weight.

Heat Pipes have been investigated as thermal vector in BTMS but not yet employed in commercially available vehicle. Table 1 presents a summary of recent development on the Heat Pipe research applied to thermal management of EVs.

**Table 1.** Summary of investigation on battery TMS employing heat pipes of different types: HP – standard Heat Pipes; TS – thermosiphons; PHP – Pulsating Heat Pipe; LHP – Loop Heat Pipe; VC – Vacuum Chamber (from 2002 to May 2021).

Author	Year	Type	Comments
Wu et al. [4]	2002	HP	Heat pipes used to cool down a large battery - at discharge current 10 A, the temperature increases to 65°C.
Jang et al. [5]	2010	TS	Thermosiphons used to transfer heat from space in between the cells to a common radiator cooled down by forced convection.
Rao et al. [6]	2013	HP	Condenser of the heat pipe is cooled down via liquid; cell maximum temperature kept below 50°C if the heat generation rate is not above 50W.
Burban et al. [7]	2013	PHP	Copper PHP tested with different fluids and with different forced convection conditions at the condenser (air velocity relative to the driving cycles).
Greco et al. [8]	2014	HP	1D lumped numerical model to analyse the performance of a heat pipe embedded in the TMS for EVs.
Wang et al. [9]	2014	HP	L-shaped heat pipe sandwiched between cells and partially submerged in a liquid pool; if the cell generates less than 10W/cell, temperature can be kept below 40°C.
Tran et al. [10]	2014	HP	Different types of condenser cooling applied to the HP; amongst free convection, forced convection and chimney cooling the best was forced convection.
Rao et al. [11]	2014	PHP	Copper –acetone PHP directly sandwiched between two adjacent cells. PHP needs to be close to the battery terminal and not horizontal.
Zhao et al. [12]	2015	HP	Flat heat pipe for pouch cells cooling. Investigation found the best way of cooling the condenser of the HP as water spray wet cooling.
Ye et al. [13]	2015	HP	Heat pipe based cooling targeting 8C fast-charging - If air cooled, the heat pipe will be effective at unit level but not at the pack level.
Putra et al. [14]	2016	LHP	Copper and SS LHP applied to a battery dummy model, working fluids are alcohol, ethanol and water. Thermal resistance was 0.2 K/W.
Ye et al. [15]	2016	HP	Heat pipe with finned condenser submerged into a flowing liquid channel is used to cool down during 8C fast charging.
Shah et al. [16]	2016	HP	Heat pipe inserted in the cell gives a 2% decrease in cell energy density, given by the encumbrance of the heat pipe, but also gives significant cooling benefits.
Liu et al. [17]	2016	HP	Ultra-micro thin heat pipe in between cells –mathematical model implemented in CFD simulations validated through IR imaging.
Zou et al. [18]	2016	HP	Integrated system of thermal management comprising cooling and heating by means of a heat pump and heat pipes L-shaped indies the cell. Thermal resistance of the heat pipe is 0.87K/W in cooling and 1.11K/W in preheating.
Wang et al. [19]	2016	PHP	Copper acetone PHP coupled with paraffin PCM - Start-up temperature of PHP should be lower than melting point of PCM.
Worwood et al. [20]	2017	HP	Heat pipe to minimize the spreading in the radial direction with heat pipe and spreader disk used inside the cell – good thermal performances but reduction in energy density by 5.8% and increases the cell mass by 11.7%.
Zhao et al. [21]	2017	HP	HP embedded in PCM - HP can extend the time of phase transition process for PCM and can increase the temperature uniformity.
Huang et al. [22]	2018	HP	HP embedded in PCM and cooled down from forced convection – works better for maximum temperature reduction but worse for temperature homogeneity.
Liang et al. [23]	2018	HP	4 copper-water heat pipes, whose evaporator is submersed into a liquid coolant flow – intermittent cooling tested to save power as well.
Ye et al. [24]	2018	HP	Micro heat pipe array to minimize the temperature variation along the cell – temperature variation stays around 1°C.
Huang et al. [22]	2018	HP	Tested 3 different TMS: PCM pure; PCM + heat pipe w/air; PCM + heat pipe w/ ethyl alcohol. - after transient cycle tests results were that PCM + heat pipe works better.
Smith et al. [25]	2018	HP	Copper water heat pipe in between cells to minimize temperature distribution. Longer heat pipe to transfer heat to a cold plate cooled down by liquid - dissipate 400 W with maximum temperature of 55°C and +/- 5°C across.

Zhou et al. [26]	2018	HP	Heat pipes at the centre of battery pack - At 1C-rate discharge, compared to cooling in ambient, the maximum temperature of pack decreases 15 °C when a fan is embedded in the centre of pack.
Gou et al. [27]	2019	VC	Novel 3D vapour chamber coupled with water loop – 120% filling ratio is the optimum for this configuration.
Wang et al. [28]	2019	HP	Heat pipe for cylindrical cells, with some conduction element to improve heat transfer surface – thickness of the conduction elements more important than conduction.
Dan et al. [29]	2019	HP	Investigated effect of air (from free convection to forced convection) on a microarray of heat pipe. Maximum temperature different between the cells < 2 °C.
Liang et al. [30]	2019	HP	Heat pipes sandwiched between cells and liquid cooled. The voltage of the battery module decreases and the available capacity decreases by about 0.88%-1.17% with reducing coolant temperature by 10 °C at 5C discharge.
Putra et al. [31]	2020	HP	Heat Pipe sandwiched between PCM and cells; heat pipe decrease the battery temperature by 26.62 °C under a 60 W heat load compared to no cooling.
Zhou et al. [32]	2020	HP	Combination of immersion cooling (in porous mats filled with flame retardant liquid), heat pipe and air cooling to hinder the spread of thermal runaway. During non-TR operations, maximum temperature was limited to 47 °C.
Gan et al. [33]	2020	HP	Feasibility studied with a validated thermal network model. Compared with the natural cooling, battery temperature reduced by 14 °C in the 5 C discharge rate
Zhang et al. [34]	2020	HP	Combination of heat pipe, PCM and forced convection. The highest temperatures under 1C, 3C, and 4C discharge rates are all under 45 °C.
Behi et al. [35]	2020	HP	Experimental comparison of liquid and flat plate heat pipe, which reduced the temperature by 29.9% and 32.6%, respectively, compared to air cooling.
Yuan et al. [36]	2020	HP	Heat pipe and cold plate coupled. Investigation on effect of effect of how much heat pipe was submersed in liquid.
Jouhara et al. [37]	2020	HP	Flat heat pipe (heat mat) applied to a 16cell module. Approximately 60% of the heat generated by the cells was removed by the heat mat.
Lei et al. [38]	2020	HP	Heat pipe cooled by water spray; At 24 A, maximum temperature and maximum temperature difference drop by 29.2 °C and 8.0 °C in comparison to no cooling
Chen et al. [39]	2020	PHP	Experimental study on PHP with TiO <sub>2</sub> Nanofluids. At ambient temperature of 35 °C and discharge rate of 1C, the maximum temperature stays below 43 °C
Behi et al. [40]	2020	HP	Comparison between free convection, forced convection and heat pipe. Maximum module temperature for forced-air cooling, heat pipe, and HPCS reaches 42.4 °C, 37.5 °C, and 37.1 °C.
Kleiner et al. [41]	2021	HP	Heat pipes used for terminal cooling in addition to conventional bottom cooling. Jelly roll temperature decreases by a maximum of 4.3 °C.
Liang et al. [42]	2021	HP	Numerical investigation of a 168-cell battery pack cooled by a flat-heat-pipe under 5C discharging rate. Maximum temperature and temperature difference are under 50 °C and 5 °C respectively.
Yao et al. [43]	2021	HP	Energy and exergy evaluation of the effect of preset temperature on air and heat pipe coupled cooling.
Chen et al. [44]	2021	HP	Heat pipe coupled with PCM, after an optimization cycle on the thickness of the PCM, numerical results showed a temperature reduction of 30%.
Alihosseini and Shafae [45]	2021	HP	Using forced convection in the condenser section of the heat pipe, keeps temperature below 40 °C, and it also improves temperature distribution.
Abbas et al. [46]	2021	HP	Experimental Investigation on combined use of heat pipe and PCM
E et al. [47]	2021	HP	Experimental and numerical investigation on heat pipe and air cooling. Parametric investigation on the spacing.
Bernagozzi et al. [48]	2021	LHP	Experimental investigation on LHP and graphite sheets applied to a module. Compared to liquid cold plate, temperature after fast charging is 3.6 °C lower.

As presented in Table 1, lots of research was focused on standard HP, but not much on LHPs. The feasibility of using LHP as thermal vector in a BTMS for a battery module was already proven by the Authors [48]. This work aims to take the investigation a step further, towards a more realistic application, by investigating the effect of a new working fluid, 3M Novec™ 649, which was chosen for having properties desired from the automotive industry. In the next sections, some details of the thermal network model used for the Lumped Parameter Model are presented (details on the fundamentals and operations of the LHP are not discussed in this work due to the targeted audience), followed by the description of the validation procedure. Finally, numerical results comparing the results obtained with ethanol and Novec™649 as working fluid are presented.

## 2. Thermal Management System Design and Thermal Network

The proposed TMS design foresees to place a LHP at the bottom of the prismatic cell battery module (as presented in Figure 1a), which cells are sandwiched between graphite sheets, allowing for an increment of heat transfer in the x-y plane and at the same time hindering the heat transfer in the z direction. This is caused by graphite typical woven structures, which gives high thermal conductivity values on the parallel direction but minimal thermal conductivity in the normal direction. The LHP will act as thermal vector between the battery module and a remote chiller connected to the HVAC system already present in the vehicle, to reduce the complexity, number of parts and costs.

The main assumptions of the LPM are: perfect thermal contact between surfaces; neglected electrolytic convection inside the battery cells; top and sides of the cells are in contact with ambient air at room temperature; incompressible liquid in the liquid line exchanges heat with the ambient; compressible vapour in the adiabatic vapour line treated as in ideal gas. More details on the equations used in this mathematical model can be found in [48].

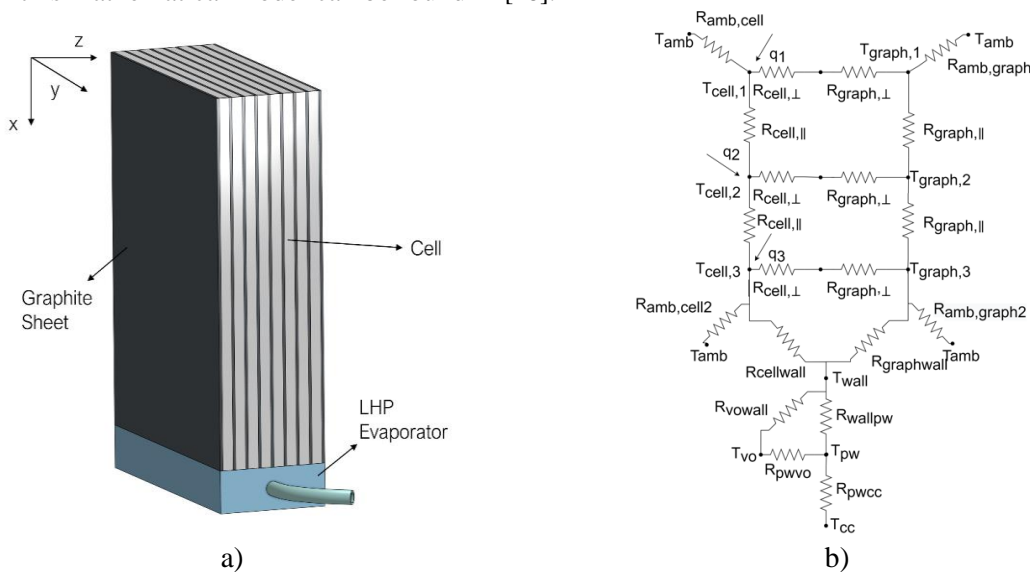


**Figure 1.** a) Schematic of the Loop Heat Pipe and Graphite BTMS and b) BTMS thermal network.

## 3. Experimental test-rig for validation

In the experimental set up, which schematic is provided in Figure 2, the battery module is composed of dummy cells, made from 5083-O aluminium plates having the same dimension as the considered cell type (presented in The use of dummy cells is a proven practice already used in literature [11] that allows to minimize the risk of generating excessive thermal stress to a real battery cell, while still evaluating the efficiency of the cooling methods.

**Table 2** together with the graphite sheets dimensions).

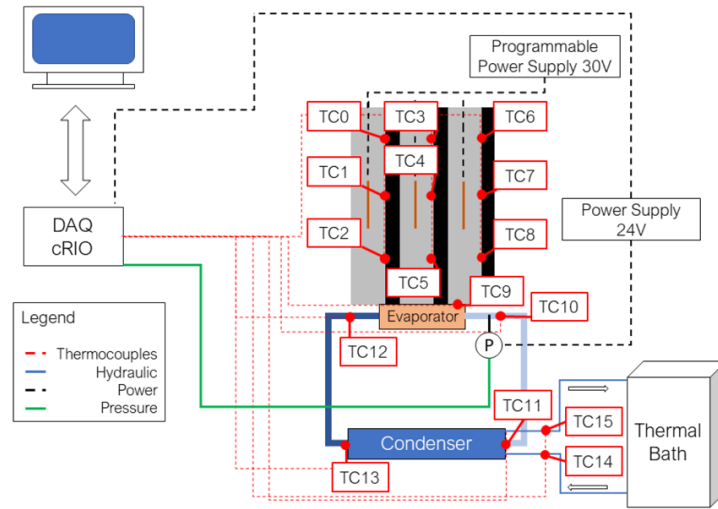


**Figure 2.** Experimental test rig with annotations.

The use of dummy cells is a proven practice already used in literature [11] that allows to minimize the risk of generating excessive thermal stress to a real battery cell, while still evaluating the efficiency of the cooling methods.

**Table 2.** Cells and graphite geometrical specifications, and physical properties used in the LPM models.

Parameter	Cell	Graphite
Thickness [mm]	10	0.8
Height [mm]	96	96
Width [mm]	280	240
Thermal Conductivity $\parallel$ [W/m·K]	46	350
Thermal Conductivity $\perp$ [W/m·K]	0.7	10
Density [kg/m <sup>3</sup> ]	3720	1300-1500
Mass Heat Capacity [J/kg·K]	1726	810
Battery Capacity [Ah]	65	-

The cells were machined to accommodate three T-type thermocouple probes each (RS PRO, SS probe, 3mm diameter, 150mm length,  $\pm 0.5^\circ\text{C}$ ) and one polyimide flexible heater (Omega KHLVA-105, 7.8  $\mu\text{m}$  thickness, 10 W/in<sup>2</sup>, 50 W), respectively. The three heaters replicate the heat generation rate profile of the cells depending on their utilization and they are powered by a programmable power supply (TENMA 72-2710, 30V, 5 A), which is controlled by a bespoke LabVIEW software. The LHP used in the present experimental campaign had wick, evaporator envelope and piping made in copper. The LHP evaporator was obtained from Thercon, Russia, and the rest of the LHP was completed in-house. This was then instrumented with a pressure transducer (Omega PXM319, 0-7 bar range, 0.25% FS BSL accuracy) fitted directly in the vapour line and 6 T-type thermocouples measuring the temperature of the external surface of the copper pipes, as shown in Figure 3. The condenser is a tube in tube heat exchanger connected to a thermal bath (Fisherbrand™ Isotemp 5150 R28, cooling capacity 500W) running DI water. The geometry of the utilized LHP is detailed in Table 3.

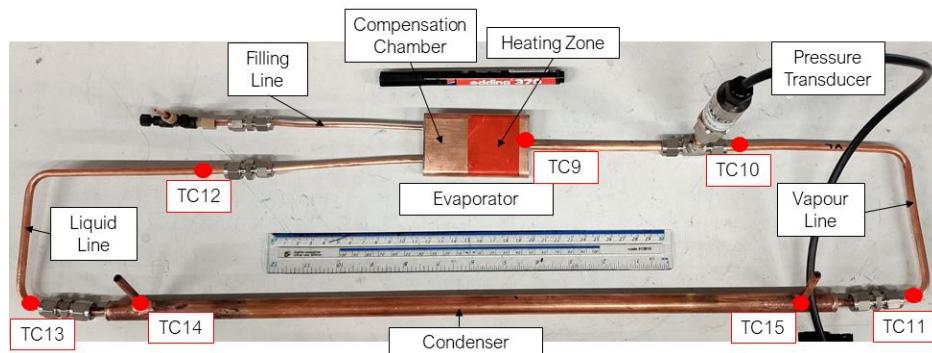


**Figure 3.** Copper/copper LHP with parts description and thermocouple numbering and positioning.

**Table 3.** Geometry of the LHP used in the present investigation (all parts are made in copper).

Part	Value	Units	Part	Value	Units		
Condenser HEX	ID/OD	4.4/6	mm	Wick	Thickness	8	mm
	ID/OD	15/11	mm		Width	45	mm
	Length	580	mm		Length	50.5	mm
			Porosity		45%		
Liquid Line	ID/OD	4.4/6	mm	Pore Size	7.3	$\mu\text{m}$	
	Length	390	mm	Evaporator Shell	Thickness	1	mm
Vapour Line	ID/OD	4.4/6	mm		Width	50	mm
	Length	400	mm		Length	84	mm
Vapour Grooves	Radius	1.5	mm	Compensation Chamber	Thickness	8	mm
	N	9	-		Width	50.5	mm
	Length	43	mm		Length	24	mm

#### 4. System validation

Validation at system level involved reproducing the results of a custom-made driving cycle test, focused on the fast charging (it involved two highway driving sections interspersed by one fast charging section). The fast charging brought the SOC of the cells from 20% to 80% in 10 minutes. Since the lumped parameter methodology carries some intrinsic limitations due to its main assumptions, a 3°C average discrepancy between experimental and numerical results is considered an acceptable value. The set temperature for the condenser was 20°C.

The graph in Figure 4 compares the average temperature of the cell nodes obtained during the experimental tests and the numerical simulations, respectively. For clarity purposes, the graph shows only the average temperature of the three thermocouple measurements as well as the average value of the three nodes for the numerical side.

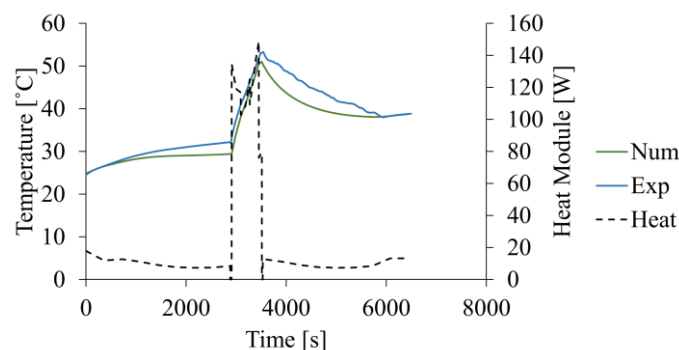


**Figure 4.** Comparison between experimental and numerical results: shown is the average cell temperature during the bespoke driving cycle.

Figure 4 shows that there is an excellent agreement between experimental and numerical data, even with a complex driving cycle. Maximum temperature is 56.7°C for the numerical and 57.9°C results, giving a difference between the experimental temperature and the numerical prediction of only 2.3°C at

the end of fast charging, which is below the indicated threshold. This gave enough confidence that the validation process was successful. More details on validation on every subsystems of the LPM can be found in [48].

The maximum temperature in the results presented in Figure 4 is above the desired threshold identified in the Introduction section, due to the mismatch between the available heating surface of the LHP evaporator and the footprint of the 3-cell module (from The use of dummy cells is a proven practice already used in literature [11] that allows to minimize the risk of generating excessive thermal stress to a real battery cell, while still evaluating the efficiency of the cooling methods).

**Table 2** and Table 3, the surfaces are  $2.3 \cdot 10^{-3} \text{ m}^2$  for the evaporator and  $8.5 \cdot 10^{-3} \text{ m}^2$  for module, giving only a 27% of coverage). The evaporator choice was limited by the manufacturer availability. However despite this, the experimented showed that the maximum  $\Delta T$  between top and bottom of the cell was  $1.2^\circ\text{C}$  and the maximum  $\Delta T$  between the cells of the module was  $4^\circ\text{C}$ , hence still fulfil two out of the three requirements highlighted in the Introduction section (cell and module levels).

To get clarity on the potential of fulfil the remaining requirement (pack level), the LPM has been employed to investigate the thermal performance of the system in the case where the heating zone of the evaporator would cover the 100% of the module footprint.

## 5. Results

As mentioned in the introduction, the working fluid selection is of paramount important not only for the performance of the TMS, but also to ensure safety of the system and passengers as well as not present a threat to the environment. As such, 3M Novec<sup>TM</sup> 649 was chosen as this working fluid is non-toxic, non-flammable, inert, dielectric, extremely low GWP of 1 and ODP of 0. Moreover, it has low freezing point ( $-108^\circ\text{C}$ ) and its boiling point ( $49^\circ\text{C}$ ) is lower than other standards working fluid used in two-phase passive devices. It was chosen to use ethanol as benchmark fluid since it already proved to be a well-performing working fluid in LHP standalone applications. Moreover, thanks to the validated LPM, it was possible to move an additional step towards the automotive industry requests, by simulating the thermal behaviour of the system if the LHP (filled with Novec<sup>TM</sup> 649) was built in aluminium, hence reducing the overall weight. The comparison is drawn over the average nodes' temperatures during the same driving cycle used in the validation process. As previously mentioned in this work, in the results presented in Figure 5 the evaporator heating zone geometry matches the module footprint.

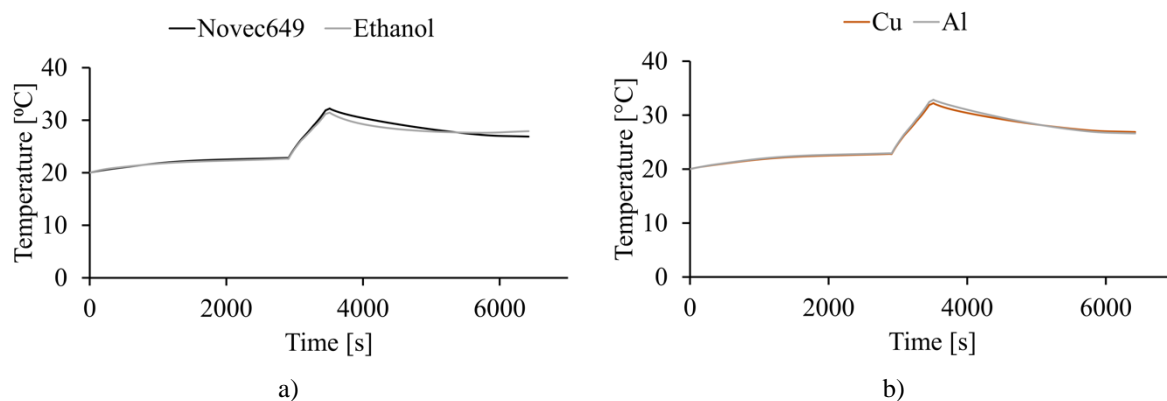


**Figure 5.** Comparison of the results using a) ethanol and Novec<sup>TM</sup> 649 in the copper LHP and b) using Novec<sup>TM</sup> 649 in a LHP made in copper and aluminum, respectively.

Results of Figure 5a show how much the module footprint coverage affects the maximum cell temperature. In fact, in this case, maximum temperature is  $32.2^\circ\text{C}$  for Novec<sup>TM</sup> 649 and  $31.5^\circ\text{C}$  for ethanol, providing an exceptional cooling performance for fast charging. Results show that the two fluids perform in a similar fashion, with maximum temperature at the end of fast charging being only  $0.8^\circ\text{C}$  different in the two cases. Novec<sup>TM</sup> 649 looks slightly better in reducing the temperature in the final highway driving section, giving a final temperature  $1^\circ\text{C}$  lower than the other fluid. This could be indicated by the lower boiling point of the 649, which allows for further temperature reduction at lower

powers. However, the take home message of the comparison graph of Figure 5a is that using Novec™ 649 provides a non-flammable, environmentally friendly and non-toxic alternative to classical heat transfer fluids, without a noticeable decrease in thermal performance. From Figure 5b, it is evident how the strong transient nature of the fast charging phenomenon and the thermal inertia involved (as previously shown in [48]), are not allowing the system to reach steady state and hence to reach sensible temperature difference. Hence the temperature difference obtaining by using a Copper LHP or an Aluminum LHP is only 0.6°C, at a gain of 70% less mass.

## 6. Conclusions

A BTMS using LHP at the bottom of a 3-cell module and graphite sheets sandwiched between the cells is applied to a 3-cell module. The idea is that the LHP transfers efficiently the heat from the module to a remote heat exchanger, connected to the HVAC chiller, already present in the vehicle, reducing the complexity of integration and number of parts. Due to the passive nature of LHP, it does so without consuming additional parasitic heat. The graphite inserts allowed efficient uniform heat transfer on the side surface of the cell, thanks to its high values of thermal conductivity. A LPM was developed to study the problem. The conclusions are as follows:

- The LPM was successfully validated by an experimental demonstrator, as the maximum temperature difference after fast charging between experiment and numerical prediction was 2.3°C.
- The BTMS proposed herein showed potential to be very efficient in containing the maximum temperature of the cells after fast charging, as numerical simulations reported a maximum temperature of 31.5°C with a LHP running ethanol and featuring a flat evaporator with an active zone the same size of the module footprint.
- The use of an alternative heat transfer fluid Novec™ 649 results in a negligible difference in thermal performance, while eliminating the flammability and toxicity issues as well as possessing desirable environmental properties such as GWP = 1 and ODP = 0.
- To use a much lighter material for the LHP, such as Aluminum, does not lead to performance detriment, as maximum temperature between the copper case is 0.6°C.

Future developments will target the experimental investigation of the system using a LHP running on Novec™ 649, to characterize even further the use of this novel working fluid.

## Acknowledgments

The Authors would like to acknowledge Ricardo plc, the Advanced Engineering Centre and the School of Computing, Engineering and Mathematics at the University of Brighton for the financial support. Finally, the Authors would like to thank Prof. Yury Maidanik and Dr. Arkadiy Ivanov from Thercon, for their overall support and guidance.

## References

- [1] Noel L, Zarazua de Rubens G, Sovacool B K and Kester J 2019 *Energy Res. Soc. Sci.* **48** 96–107
- [2] Ma S, Jiang M, Tao P, Song C, Wu J, Wang J, Deng T and Shang W 2018 *Prog. Nat. Sci. Mater. Int.* **28** 653–66
- [3] Feng X, Ouyang M, Liu X, Lu L, Xia Y and He X 2018 *Energy Storage Mater.* **10** 246–67
- [4] Wu M S, Liu K H, Wang Y Y and Wan C C 2002 **109** 160–6
- [5] Jang J-C and Rhi S 2010 *US-Korea Conf. Sci. Technol. Entrep.* **110** 2
- [6] Rao Z, Wang S, Wu M, Lin Z and Li F 2013 *Energy Convers. Manag.* **65** 92–7
- [7] Burbán G, Ayel V, Alexandre A, Lagonotte P, Bertin Y and Romestant C 2013 *Applied Thermal Engineering* vol 50 pp 94–103

- [8] Greco A, Cao D, Jiang X and Yang H 2014 *J. Power Sources* **257** 344–55
- [9] Wang Q, Jiang B, Xue Q F, Sun H L, Li B, Zou H M and Yan Y Y 2014 *Appl. Therm. Eng.* **88** 54–60
- [10] Tran T-H, Harmand S and Sahut B 2014 *J. Power Sources* **265** 262–72
- [11] Rao Z, Huo Y and Liu X 2014 *Exp. Therm. Fluid Sci.* **57** 20–6
- [12] Zhao R, Gu J and Liu J 2015 *J. Power Sources* **273** 1089–97
- [13] Ye Y, Saw L H, Shi Y and Tay A A O 2015 *N Appl. Therm. Eng.* **86** 281–91
- [14] Putra N, Ariantara B and Pamungkas R A 2016 *Appl. Therm. Eng.* **99** 784–9
- [15] Ye Y, Shi Y, Saw L H and Tay A A O 2016 *Int. J. Heat Mass Transf.* **92** 893–903
- [16] Shah K, McKee C, Chalise D and Jain A 2016 *Energy* **113** 852–60
- [17] Liu F, Lan F and Chen J 2016 *J. Power Sources* **321** 57–70
- [18] Zou H, Wang W, Zhang G, Qin F, Tian C and Yan Y 2016 *Energy Convers. Manag.* **118** 88–95
- [19] Wang Q, Rao Z, Huo Y and Wang S 2016 *Int. J. Therm. Sci.* **102** 9–16
- [20] Worwood D, Kellner Q, Wojtala M, Widanage W D, McGlen R, Greenwood D and Marco J 2017 *J. Power Sources* **346** 151–66
- [21] Zhao J, Lv P and Rao Z 2017 *Exp. Therm. Fluid Sci.* **82** 182–8
- [22] Huang Q, Li X, Zhang G, Zhang J, He F and Li Y 2018 *E Appl. Therm. Eng.* **141** 1092–100
- [23] Liang J, Gan Y and Li Y 2018 *Energy Convers. Manag.* **155** 1–9
- [24] Ye X, Zhao Y and Quan Z 2018 *Appl. Therm. Eng.* **130** 74–82
- [25] Smith J, Singh R, Hinterberger M and Mochizuki M 2018 *Int. J. Therm. Sci.* **134** 517–29
- [26] Zhou S, Zhao Q, Yan K, Li Y, Wang Y, Wang G, Feng L and Luo C 2018 *J. Energy Storage* **16** 84–92
- [27] Gou J and Liu W 2019 *Appl. Therm. Eng.* **152** 362–9
- [28] Wang J, Gan Y, Liang J, Tan M and Li Y 2019 *Appl. Therm. Eng.* **151** 475–85
- [29] Dan D, Yao C, Zhang Y, Zhang H, Zeng Z and Xu X 2019 *Appl. Therm. Eng.* **162** 114183
- [30] Liang J, Gan Y, Li Y, Tan M and Wang J 2019 *Energy* **189** 116233
- [31] Putra N, Sandi A F, Ariantara B, Abdullah N and Indra Mahlia T M 2020 *Case Stud. Therm. Eng.* **21** 100655
- [32] Zhou H, Dai C, Liu Y, Fu X and Du Y 2020 *J. Power Sources* **473** 228545
- [33] Gan Y, Wang J, Liang J, Huang Z and Hu M 2020 *Appl. Therm. Eng.* **164** 114523
- [34] Zhang W, Qiu J, Yin X and Wang D 2020 *Appl. Therm. Eng.* **165** 114571
- [35] Behi H, Karimi D, Behi M, Jaguemont J, Ghanbarpour M, Behnia M, Berecibar M and Van Mierlo J 2020 *J. Energy Storage* **32** 101893
- [36] Yuan X, Tang A, Shan C, Liu Z and Li J 2020 *J. Energy Storage* **32** 101984
- [37] Jouhara H, Serey N, Khordehgah N, Bennett R, Almahmoud S and Lester S P 2020 *Int. J. Thermofluids* **1–2** 100004
- [38] Lei S, Shi Y and Chen G 2020 *Int. J. Heat Mass Transf.* **163** 120494
- [39] Chen M and Li J 2020 *J. Energy Storage* **32** 101715
- [40] Behi H, Karimi D, Behi M, Ghanbarpour M, Jaguemont J, Sokkeh M A, Gandoman F H, Berecibar M and Van Mierlo J 2020 *Appl. Therm. Eng.* **174** 115280
- [41] Kleiner J, Singh R, Schmid M, Komsiyyska L, Elger G and Endisch C 2021 *Appl. Therm. Eng.* **188** 116328
- [42] Liang Z, Wang R, Malt A H, Soury M, Esfahani M N and Jabbari M 2021 *Appl. Therm. Eng.* **192** 116934
- [43] Yao M, Gan Y, Liang J, Dong D, Ma L, Liu J, Luo Q and Li Y 2021 *Appl. Therm. Eng.* **191**
- [44] Chen K, Hou J, Song M, Wang S, Wu W and Zhang Y 2021 *Appl. Therm. Eng.* **188** 116665
- [45] Alihosseini A and Shafae M 2021 *J. Energy Storage* **39** 102616
- [46] Abbas S, Ramadan Z and Park C W 2021 *Int. J. Heat Mass Transf.* **173** 121269
- [47] E J, Yi F, Li W, Zhang B, Zuo H, Wei K, Chen J, Zhu H, Zhu H and Deng Y 2021 *Energy* **226** 120336
- [48] Bernagozzi M, Georgoulas A, Miché N, Rouaud C and Marengo M 2021 *Appl. Therm. Eng.* **194**